accepted for publication in ApJ
Preprint typeset using LaTeX style emulateapj v. 5/2/11

PROBING THE PARSEC-SCALE ACCRETION FLOW OF 3C 84 WITH MILLIMETER POLARIMETRY

R. L. Plambeck[1], G. C. Bower[2], Ramprasad Rao[2], D. P. Marrone[3], S. G. Jorstad[4,5], A. P. Marscher[4], S. S. Doeleman[6,7], V. L. Fish[6], M. D. Johnson[7]

accepted for publication in ApJ

ABSTRACT

We report the discovery of Faraday rotation toward radio source 3C 84, the active galactic nucleus in NGC1275 at the core of the Perseus Cluster. The rotation measure (RM), determined from polarization observations at wavelengths of 1.3 and 0.9 mm, is $(8.7 \pm 2.3)\times 10^5$ rad m^{-2}, among the largest ever measured. The RM remained relatively constant over a 2 year period even as the intrinsic polarization position angle wrapped through a span of 300 degrees. The Faraday rotation is likely to originate either in the boundary layer of the radio jet from the nucleus, or in the accretion flow onto the central black hole. The accretion flow probably is disk-like rather than spherical on scales of less than a parsec, otherwise the RM would be even larger.

Subject headings: accretion, accretion disks — polarization — galaxies: active — galaxies: jets — galaxies: individual(3C 84)

1. INTRODUCTION

Radio source 3C 84 is associated with the active galactic nucleus (AGN) in NGC 1275, the central galaxy in the Perseus cluster, the prototypical 'cooling flow' cluster (Fabian 1994). The black hole in the AGN launches powerful jets into the surrounding medium. The accretion process onto the black hole has been studied through a variety of techniques on scales as small as a few parsecs (Vermeulen et al. 1994; Walker et al. 1994, 2000; Wilman et al. 2005; Scharwächter et al. 2013). At the distance of NGC1275, 1 pc subtends 3 milliarcseconds.

At cm wavelengths 3C 84 is well-known as an 'unpolarized' calibrator. Why is this so, given that the radio emission from the AGN and its associated jet arise from synchrotron emission, which should be highly polarized? One possibility is that Faraday rotation twists the position angle χ of this linearly polarized radiation as it propagates through foreground plasma. The position angle is rotated by $\Delta\chi = \mathrm{RM}\,\lambda^2$, where RM is the rotation measure. If RM varies across the source and the observations do not resolve this structure ("beam depolarization"), the net observed polarization may be very small.

Measurements of Faraday rotation along the line of sight to the black hole provide a valuable diagnostic of the accretion flow onto the central object, since the RM is proportional to the integral of the electron density and the magnetic field along the line of sight. In the case of SgrA*, for example, the RM has been used to constrain both the mode and the rate of the accretion onto its black hole (Bower et al. 2003; Marrone et al. 2007). Similar methods have recently been applied to M87 (Kuo et al. 2014). Time variability of the RM could also be a valuable probe of turbulence in the accretion region (Pang et al. 2011).

For 3C 84, Taylor et al. (2006) found an RM of about 7000 rad m^{-2} toward a small spot in the jet about 15 milliarcseconds (~ 5 pc) south of the nucleus, based on VLBA maps at wavelengths of 1.3, 2.0, and 3.6 cm. It was not possible to fit the RM toward the nucleus itself because in that direction linear polarization was detected only at a single wavelength (and only at the 0.2% level). At 7 mm, where emission from the nucleus becomes dominant, VLBA monitoring observations by the Boston University group[8] (Marscher et al. 2011) sometimes detect spots of weak linear polarization toward the nucleus, but typically the polarized flux density is $< 0.5\%$ of the peak flux density.

Polarization should be easier to detect at mm wavelengths because Faraday rotation decreases steeply at shorter wavelengths, and because the mm emission region is smaller, so that variations in RM across the source are less problematic. However, based on observations made with the Plateau de Bure interferometer in 2011 Mar, Trippe et al. (2012) placed upper limits of 0.5% on the linear polarization of 3C 84 at wavelengths of 1.3 and 0.9 mm. Here we report observations at the same wavelengths made over a 2 year period with the Combined Array for Research in Millimeter Astronomy (CARMA) and with the Submillimeter Array (SMA). The fractional polarization of 3C 84 was $< 0.6\%$ in the earliest data, from 2011 May, consistent with the Trippe et al. (2012) results, but by late 2011 it had increased to the 1–2% level. The RM inferred from the data is $\sim 9 \times 10^5$ rad m^{-2}, among the largest ever measured. We discuss the implications of these results for the accretion flow onto the black hole in 3C 84.

plambeck@berkeley.edu
[1] Radio Astronomy Laboratory, University of California, Berkeley, CA 94720, USA
[2] Academia Sinica Institute for Astronomy and Astrophysics (ASIAA), 645 N. Aohoku Pl., Hilo, HI 96720, USA
[3] Steward Observatory, University of Arizona, 933 North Cherry Avenue, Tucson, AZ 85721, USA
[4] Institute for Astrophysical Research, Boston University, 725 Commonwealth Avenue, Boston, MA 02215, USA
[5] Astronomical Institute, St. Petersburg State University, Universitetskij Pr. 28, 198504 St. Petersburg, Russia
[6] MIT Haystack Observatory, Route 40, Westford, MA 01886, USA
[7] Harvard-Smithsonian Center for Astrophysics, 60 Garden Street, Cambridge, MA 02138, USA

[8] http://www.bu.edu/blazars/VLBAproject.html

2. OBSERVATIONS

2.1. *CARMA Observations*

The CARMA polarization system (Hull et al. 2013, 2014) consists of dual-polarization 1.3 mm receivers that are sensitive to right- (R) and left-circular (L) polarization, and a spectral-line correlator that measures all four cross-correlations (RR, LL, LR, RL) on each of the 105 baselines connecting the 15 antennas.

The double sideband receivers are sensitive to signals at sky frequencies $\nu_{\rm sky} = \nu_{\rm LO} \pm \nu_{\rm IF}$ above (upper sideband) and below (lower sideband) the local oscillator frequency $\nu_{\rm LO}$. Signals received in these two sidebands are separated in cross-correlation spectra. The correlator provides 4 independently tunable sections, each up to 500 MHz wide. Typically we centered these sections at intermediate frequencies $\nu_{\rm IF}$ of 6–8 GHz, so that the polarization data from the upper and lower sidebands spanned a sky frequency range of 16 GHz.

Data were analyzed with the MIRIAD package (Sault et al. 1995). Stokes parameters I, Q, and U were derived for each of the 8 spectral windows (4 sections $\times$ 2 sidebands). Q and U may be considered components of a complex polarization vector $p = Q + iU = p_0 \exp(i2\chi)$. Here p_0 is the linearly polarized flux density in Jy, $\chi(\nu) = \chi_0 + {\rm RM}(c^2/\nu^2 - c^2/\nu_0^2)/(1+z)^2$ is the electric vector position angle, RM is the rotation measure, z is the redshift, and χ_0 is the position angle at the reference frequency ν_0 (225 GHz). The factor $(1+z)^2$ arises because Faraday rotation takes place at frequency $\nu(1+z)$ in the source frame; this correction factor is negligible for 3C 84, at $z = 0.018$. We fit $Q(\nu)$ and $U(\nu)$ to solve for p_0, χ_0, and RM.

For a bright but weakly polarized source like 3C 84, the accuracy of the measurements is limited by systematic errors, not thermal noise. The primary difficulty is in correcting for the polarization leakages – the cross coupling between the L and R channels caused by imperfections in the receivers or crosstalk in the IF system. Leakages are derived from observations of a bright point source, polarized or unpolarized (usually 3C 84 itself), obtained over a wide range of parallactic angle. Miriad task `gpcal` fits these data to solve simultaneously for the source polarization, receiver gains, and leakage corrections. Since the CARMA receivers have no moving parts the leakages are stable over periods of months. Their magnitudes are typically of order 6%, however, and they have considerable frequency structure. We calibrated the leakages separately for each of the 8 spectral windows.

We were able to set only a crude upper limit of $\lesssim 2\%$ on the magnitude of circular polarization (Stokes V) because this requires highly accurate calibration of the gains of the R and L channels on a source other than 3C 84.

2.2. *SMA Observations*

SMA observations were conducted in both the 1.3 mm and 0.9 mm bands. The single polarization receivers are switched between R and L circular polarization by inserting quarter wave plates into the optical path. Using a different switching pattern for each of the 8 telescopes, all 4 cross-polarizations (RR, LL, LR, RL) are measured every 5 minutes on each baseline. Like CARMA, the SMA operates in double sideband mode, with a 4–8 GHz IF. The available observational bandwidths were either 2 GHz or 4 GHz. Thus the data spanned a sky frequency range of either 10 GHz or 12 GHz.

Data were reduced using a combination of the MIR/IDL and MIRIAD data reduction packages. The instrumental polarization is frequency-dependent and the typical values are $\sim 2\%$. The instrumental polarization is determined with an accuracy of $\sim 0.1\%$. The RM was fit to the difference in the upper and lower sideband position angles.

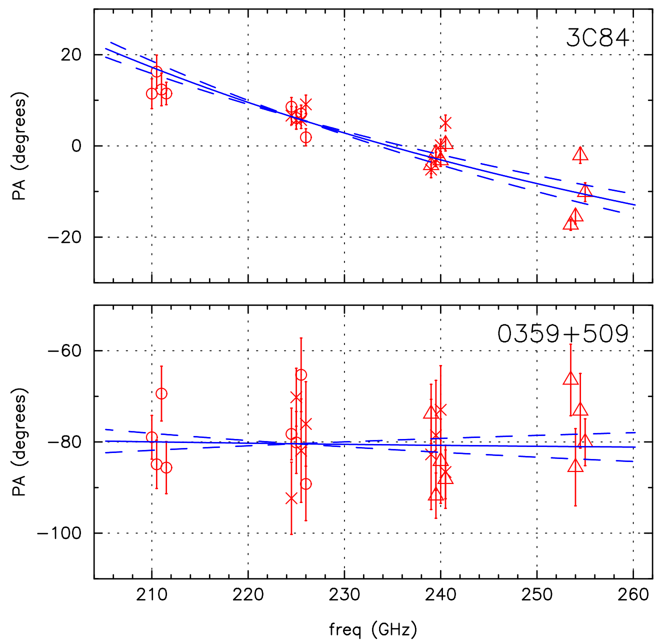

FIG. 1.— Polarization position angles from 211 to 255 GHz for 3C 84 and comparison source 0359+509 measured with CARMA on 2013 Aug 04. Symbols indicate the LO frequency used for the observations – circles, 218 GHz; crosses, 232.5 GHz; triangles, 247 GHz. The sky frequencies observed at $\nu_{\rm LO}$ of 232.5 GHz overlap those observed at 218 and 247 GHz. The error bars are estimated from the scatter in the measurements at each frequency and do not fully reflect systematic errors in the polarization leakage calibration. Fractional polarizations of 1.5% were measured for both 3C 84 and 0359+509; 0359+509 has a much lower flux density than 3C 84, so the position angle uncertainties due to thermal noise are larger. Rotation measures are derived from fits to the position angle vs. frequency, indicated by the blue curves.

3. RESULTS

The 3C 84 data reported here span the period from 2011 May through 2013 August. In almost all cases 3C 84 was observed as a calibrator for another science target. Many of the CARMA datasets were from the TADPOL survey (Hull et al. 2014).

One CARMA observation targeted 3C 84 specifically. In an 8-hour observation on 2013 August 04 we interleaved observations at LO frequencies of 218, 232.5, and 247 GHz to obtain wide parallactic angle coverage at 16 sky frequencies from 210–255 GHz. Both 3C 84 and a comparison calibrator, 0359+509, were observed. Fits to these data, shown in Figure 1, give RM of $(7 \pm 1) \times 10^5$ rad m^{-2} for 3C 84 and $(1.9 \pm 7.6) \times 10^5$ rad m^{-2} for 0359+509. The uncertainty is large for 0359+509 because this source is at

TABLE 1
CARMA and SMA Observations of 3C 84

Epoch	ν_{LO} (GHz)	p^a (%)	χ^b (deg)	RM (10^5 rad m^{-2})
CARMA 1.3 mm				
2011May03	223.8	0.6	-63 ± 8	-14.0 ± 19.0
2011Oct27	223.8	1.2	-56 ± 2	9.8 ± 3.0
2011Nov09	223.8	1.3	-59 ± 2	7.9 ± 2.9
2012Apr07	223.8	1.2	-76 ± 3	9.1 ± 3.7
2012Jun24	223.8	1.5	40 ± 1	11.0 ± 2.1
2012Jul30	223.8	1.0	13 ± 2	14.1 ± 2.4
2012Sep02	223.8	1.5	-13 ± 1	10.6 ± 1.2
2012Oct18	223.8	1.0	-41 ± 2	8.5 ± 3.0
2012Oct30	223.8	0.8	-49 ± 4	8.9 ± 4.7
2012Nov24	223.8	1.2	-86 ± 2	7.0 ± 3.1
2013Mar22	226.3	1.4	43 ± 1	10.6 ± 2.3
2013Mar23	226.3	1.4	29 ± 2	8.1 ± 4.3
2013Aug04	232.5	1.5	5 ± 1	7.0 ± 0.9
SMA 1.3 mm				
2012Jun24	224.9	2.5	34 ± 1	7.2 ± 1.7
2012Jul20	226.9	1.4	12 ± 1	7.6 ± 2.7
2012Sep07	224.9	1.8	-14 ± 1	5.9 ± 2.1
2013Jan23	225.3	1.5	73 ± 1	3.7 ± 2.6
2013Jul05	226.9	3.2	61 ± 1	10.5 ± 1.2
2013Aug15	226.9	1.4	12 ± 1	8.4 ± 3.0
SMA 0.9 mm				
2011Aug20	341.7	2.2	85 ± 3	6.4 ± 20.6
2012Jun15	343.0	2.0	4 ± 2	16.3 ± 13.8
2012Jul03	340.1	1.5	-9 ± 1	0.0 ± 8.9
2012Aug08	340.1	1.4	-38 ± 2	9.4 ± 15.7
2012Sep02	340.8	2.0	-46 ± 3	3.2 ± 17.9
2012Oct14	341.4	1.5	-67 ± 1	9.6 ± 9.1
2013Feb01	341.6	0.6	32 ± 4	-22.5 ± 22.8
2013Aug25	341.6	1.4	-20 ± 2	-9.7 ± 11.6

[a] Fractional polarizations were *not* corrected for noise bias, since the polarized flux density was typically more than 10 times the thermal noise level.
[b] Polarization position angles χ are interpolated to 225 GHz for the 1.3 mm data, and to 341 GHz for the 0.9 mm data.

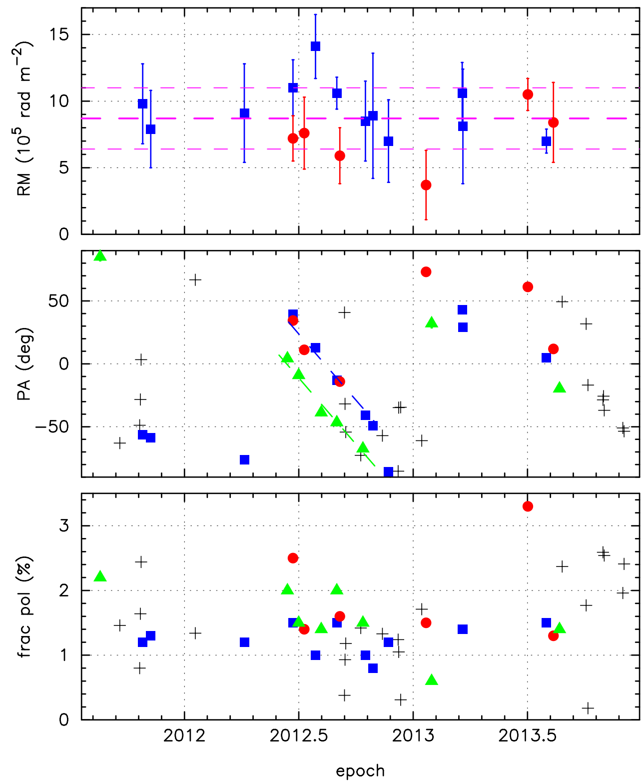

Fig. 2.— Polarized intensities, electric vector position angles, and rotation measures observed at 1.3 mm (blue squares, CARMA; red circles, SMA) and 0.9 mm (green triangles, SMA) from 2011 Aug through 2013 Dec. Optical fractional polarizations and position angles measured at Lowell Observatory are shown by black crosses. The dashed lines in the middle panel show that in mid-2012 the position angles at 0.9 mm were roughly 35° more negative than those at 1.3 mm, consistent with a rotation measure of 6×10^5 rad m^{-2}. Dashed lines in the top panel show the mean ± 1 standard deviation of the 1.3 mm RM measurements.

redshift z=1.52, and the RM scales as $(1+z)^2$; however, the 0359+509 data rule out the possibility that the systematic 25° position angle variation measured for 3C 84 could be an instrumental effect.

The fractional polarizations, position angles, and rotation measures derived from all observations are summarized in Table 1 and plotted in Figure 2. In our earliest data, from 2011 May, the fractional polarization of 3C 84 was very low, $\lesssim 0.6\%$, but for most of the following observations it was in the 1–2% range. The polarization position angle trended monotonically toward more negative values, apparently wrapping through from $-90°$ to $+90°$ twice over the 2 year span of the observations.

Also plotted in Figure 2 are the R-band optical polarizations and position angles for 3C 84 measured with the 1.8-m Perkins telescope at Lowell Observatory (Flagstaff, AZ) using the PRISM camera. The observations and data reduction were performed in the same manner as described by Jorstad et al. (2010) for the quasar 3C454.3. The 1–2% fractional polarization in the optical is similar to that at mm wavelengths, but there is not a simple correspondence between the optical and mm position angles; χ_{opt} sometimes fluctuates by tens of degrees on time scales of days, while χ_{mm} tends to vary more smoothly.

Generally there is good agreement between the CARMA and SMA results at 1.3 mm; significant RM measurements were made with both instruments. It was not possible to detect Faraday rotation from the 0.9 mm data alone – at this wavelength the expected position angle difference between the upper and lower sidebands is only 2.5° for an RM of 10^6 rad m^{-2}. However, interpolation of the data in Figure 2 shows that position angles at 0.9 mm were 30–40° more negative than those at 1.3 mm in mid-2012. The fact that this offset is maintained over a period of months even as the position angles at both wavelengths rotate through 90 degrees provides powerful evidence that we are observing Faraday rotation in an external screen, rather than variations in the polarization direction vs. synchrotron optical depth. A $35° \pm 5°$ difference in the 1.3 mm and 0.9 mm position angles corresponds to an RM of $(6 \pm 1) \times 10^5$ rad m^{-2}.

The uncertainties in the RM measurements listed in Table 1 do not fully account for possible systematic errors in the polarization leakage corrections. Thus, although our results allow for possibility of up to 50% variations in the RM on time scales of days or weeks, the evidence for such variations is not convincing. An average of the 1.3 mm RM values, excluding the anomalous result from 2011 May, gives RM = $(8.7 \pm 2.3) \times 10^5$ rad m^{-2}, where the uncertainty is the standard deviation of the measurements.

4. INTERPRETATION

Where do the linearly polarized emission and Faraday rotation originate in 3C 84, and what conclusions can we draw about the source?

4.1. *Source of the polarized emission*

We expect that at wavelengths of $\lesssim 1.3$ mm most of the flux originates from a small region, probably less than a milliarcsecond ($\lesssim 0.4$ pc) across, centered close to the nucleus. For an AGN with radio jets the mm emission "core" is thought to be located somewhere in the approaching jet, displaced from the black hole.

In blazars, where the jet is closely aligned with our line of sight, the core may be offset by thousands of Schwarzschild radii (R_S) from the black hole, near the end of the zone where the jet is electromagnetically accelerated, because this is where Doppler boosting is greatest. For jets that are viewed at a substantial angle, however, this model predicts that the core should be close to the base of the jet (Marscher 2006). In M87, for example, where the jet is inclined by $\sim 20°$ with respect to the line of sight, VLBA observations by Hada et al. (2011) show that the 7 mm radio core is offset by only 14–23 R_S from the black hole, while 1.3 mm VLBI observations appear to resolve the base of the jet, just 2.5–4 R_S from the black hole (Doeleman et al. 2012). The jets in 3C 84 are mildly relativistic ($0.3c - 0.5c$) and are directed at an angle of roughly 30° to 55° to the line of sight (Walker et al. 1994; Asada et al. 2006), so here too the offset of the core from the black hole may be small.

Variations in the polarization position angle presumably are caused by changes in the magnetic field structure of the emitting region, possibly as the result of shocks propagating along the jet similar to what is seen in blazars (e.g., Aller et al. 1999). Optical emission originates in these same shocks, although from volumes that are much smaller, leading to faster fluctuations in the optical position angles (Jorstad et al. 2010). The rotation of 3C 84's optical and mm polarization position angles with time is reminiscent of the systematic variations seen in BL Lac in late 2005. In BL Lac, this rotation was correlated with an optical, X-ray, and radio outburst, and was attributed to a shock propagating along a helical magnetic field in the jet (Marscher et al. 2008).

4.2. *Location of the Faraday screen*

Where, then, is the Faraday screen? Is it close to the nucleus, or far away in the intracluster gas? The rotation measure is given by (Gardner & Whiteoak 1966)

$$RM = 8.1 \times 10^5 \int n_e \, \mathbf{B} \cdot d\ell \quad \text{radians m}^{-2},$$

where n_e is the thermal electron density in cm^{-3}, $\mathbf{B}$ is the magnetic field in gauss, and $d\ell$ is the path length along the direction of propagation in pc. Only the component of the magnetic field along the line of sight contributes; if the field is tangled, with many reversals along the line of sight, the RM will be reduced.

It is implausible that the Faraday rotation originates in the intracluster gas. Typical RMs toward cooling flow clusters are in the range 10^3 to 10^4 rad m^{-2} (Carilli & Taylor 2002), similar to the RM of 7000 rad m^{-2} measured by Taylor et al. (2006) 15 mas (5 pc) from 3C 84's nucleus. The RM could be higher if we happen to view the nucleus along the axis of one of the partially ionized filaments that thread the intracluster gas surrounding NGC1275 (Conselice et al. 2001). These filaments, $\lesssim 70$ pc in diameter and several kpc long, are stabilized by 10^{-4} gauss magnetic fields (Fabian et al. 2008). If our line of sight to the nucleus passed precisely along the axis of such a filament it could account for the measured RM, but such perfect alignment is improbable.

Probably the Faraday screen is close to the nucleus, within a parsec of the emission core. We cannot be certain whether the material in this screen is being blown out from the black hole or is accreting onto it. We consider these two possibilities below.

4.3. *Faraday rotation in the jet boundary layer?*

Faraday rotation might originate in the sheath or boundary layer of the radio jet, in plasma that is flowing outward from the black hole. Zavala & Taylor (2004) suggested such a geometry to explain the Faraday rotation measured in a sample of 40 radio galaxies and quasars observed with the VLBA at wavelengths of 2 cm to 3.6 cm. Rotation measures were typically 10^3 to 10^4 rad m^{-2} for the radio cores in these sources. This is comparable to the RM of about 7000 rad m^{-2} measured in the 3C 84 jet 5 pc from the nucleus by Taylor et al. (2006) at wavelengths of 1.3 to 3.6 cm. The much higher RM that we measure at 1.3 mm might be explained if the mm emission originates closer to the base of the jet and thus propagates through a denser zone of the boundary layer.

In fact, an increase of RM at shorter wavelengths appears to be common in radio jets. In an AGN polarization survey, Jorstad et al. (2007) found that the RM measured at mm wavelengths was greater than the RM measured at cm wavelengths in 8 of 8 sources; a fit to these data gave $|\mathrm{RM}(\lambda)| = \lambda^{-a}$, with $a = 1.8 \pm 0.5$. This dependence can be explained by a simple model in which the $\tau \sim 1$ surface is located at distance $d \propto \lambda$ along the jet, and where the magnetic field, path length, and electron density in the boundary layer scale as d^{-1}, d, and d^{-2} respectively, giving $|\mathrm{RM}(\lambda)| \propto \lambda^{-2}$ (Jorstad et al. 2007).

For 3C 84, scaling the 1.3 cm RM of 7000 rad m^{-2} by λ^{-2} gives RM $\sim 7 \times 10^5$ rad m^{-2} at 1.3 mm, in good agreement with the measured value. We caution that this agreement may be a fortuitous coincidence. The model assumes that the cm emission originates 10 times farther from the nucleus than does the mm emission. In fact, however, the mm emission likely originates within a few $\times$ 0.1 mas of the nucleus, whereas the cm RM was measured at the tip of the jet 15 mas away, so the actual distance ratio is closer to 100.

4.4. *Faraday rotation in the accretion flow?*

We now consider the possibility that the Faraday rotation originates in the accretion flow onto the black hole. The RM, $\sim 9 \times 10^5$ rad m^{-2}, is among the largest ever detected. However, it is striking for the fact that it is not larger. It is less than a factor of two greater than the RM observed toward SgrA*, which is thought to originate in a radiatively inefficient accretion flow (RIAF) surrounding the black hole (Bower et al. 2003; Marrone et al. 2007). For SgrA* the RM constrains the accretion rate onto the

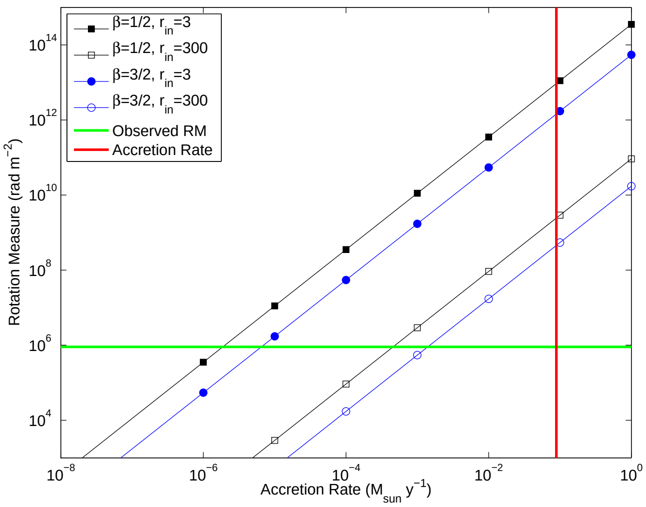

FIG. 3.— Rotation measure vs. accretion rate for 3C 84 predicted by radiatively inefficient accretion flow models. The RM depends on β, the density power law index ($n(r) \propto r^{-\beta}$), and r_{in}, the radius where the electrons become relativistic, given in units of the Schwarzschild radius R_S. The accretion rate is the mass inflow rate at r_{in}. The horizontal green line indicates the measured RM; the vertical red line indicates the accretion rate estimated from the bolometric luminosity and a 10% radiation efficency. These spherically symmetric models fit the measured RM only if an unrealistically large value for r_{in} is assumed.

black hole to be $\lesssim 10^{-7}\ M_\odot\, y^{-1}$; Bondi accretion is excluded because it requires an even higher RM. Accretion onto the black hole in 3C 84, on the other hand, powers a massive outflow into the Perseus Cluster. In 3C 84 the black hole mass is $8\times10^8\, M_\odot$ (Scharwächter et al. 2013), 2.5 orders of magnitude larger than SgrA*, and the total luminosity is 4×10^{44} erg s^{-1} (Levinson et al. 1995), 9 orders of magnitude larger. If the RM scales with the black hole mass or mass accretion rate, we might expect it to be orders of magnitude larger in 3C 84.

Accretion flow models fall into two classes. RIAF models should be applicable to sources with luminosities less than about 1% of the Eddington luminosity (Narayan et al. 2012); thin disk models (Shakura & Sunyaev 1973) are more appropriate for higher luminosity sources. 3C 84's luminosity is about 0.4% of its Eddington luminosity of $\sim 10^{47}$ ergs s^{-1}, so it is reasonable to use RIAF models to predict its RM.

Following the formulation for the RM as a function of accretion rate for spherical power-law accretion profiles in Marrone et al. (2006)[9], we calculated the RM for RIAF models with inner radii r_{in} of 3 and 300 Schwarzschild radii R_S (Figure 3). $R_S = 8\times10^{-5}$ pc for an $8\times10^8\, M_\odot$ black hole; r_{in} is the radius at which the accretion flow becomes relativistic, or is truncated for some other reason. We assume a very large outer radius, $r_{out} \sim 10^5\, R_S$, about 8 pc. The results are not sensitive to r_{out} or to the density power-law index, β, which selects between the limiting cases of advection-dominated accretion flow (ADAF; $\beta = 3/2$) and convection-dominated accretion flow (CDAF; $\beta = 1/2$) models.

For $r_{in} = 3R_S$ the measured RM implies an accretion rate $\lesssim 10^{-6} M_\odot\,$y^{-1}. This value is strongly inconsistent with the accretion rate $\dot{M} \sim L/(0.1\,c^2) \sim 10^{-1} M_\odot\,$y^{-1} estimated from the bolometric luminosity and a radiative efficiency of 10%; an even higher accretion rate is required if the radiative efficiency is lower. We can account for the RM in an ADAF context only if $r_{in} = 3000R_S \sim 0.2$ pc. Even larger values are required for CDAF models. But these inner radii are much larger than any theoretical expectations. If the polarized radiation at 1.3 mm originates close to the black hole, then either the magnetic field in the accretion flow is much weaker than the equipartition value assumed in the calculation, or the field is highly tangled, or the accretion flow is disk-like rather than spherical.

Other observations suggest that material close to the nucleus of NGC1275 lies in a disk that is tilted with respect to the line of sight. For example, Scharwächter et al. (2013) model NIR observations of ionized species in the inner 1.5″ (50 pc) region as originating from a disk at an inclination angle of 45°, with electron density $n_e \sim 4\times10^3$ cm^{-3} and temperature $T_e \sim 15000$ K.

This disk is detectable on even smaller scales via radio free-free absorption in multifrequency VLBA images (Walker et al. 1994, 2000). Absorption is seen against the N counterjet, but not toward the nucleus or the S jet. Modeling suggests that it originates in a torus with $n_e \sim 10^4$ cm^{-3}, $T_e \sim 10^4$ K, and $L \sim 3$ pc (Levinson et al. 1995). The equipartition magnetic field in this gas is $B_{eq} = 4(\pi n_e kT)^{1/2} \sim 0.8$ mG. If the polarized mm emission passed through 3 pc of this material, the RM could be as large as 2×10^7 rad m^{-2}, 20 times the measured value. Probably line of sight to the mm core intercepts only a small fraction of this material. Since we do not know the exact location of the mm emission region relative to the black hole, it is difficult to constrain the scale height of the disk.

The absence of measurable free-free absorption toward the nucleus at 1.3 cm can be explained if the cm wavelength emission originates farther downstream in the jet due to optical depth effects, as in the model described in Section 4.3 above.

The jet efficiency, $\eta_{\rm jet}$, defined as the ratio of the jet power $P_{\rm jet}$ to the accretion power $\dot{M}_{BH}c^2$ onto the black hole, has been used to explore the mechanisms through which jets are launched, as well as the role of black hole spin and magnetic fields (e.g., Nemmen & Tchekhovskoy 2014). $P_{\rm jet}$ may be inferred from the energetics of X-ray cavities excavated by the jets. If one assumes that accretion onto the black hole occurs at the Bondi rate, then it is typical to infer jet efficiencies of a few percent (Allen et al. 2006). Bondi accretion is spherically symmetric inflow from the accretion radius $r_B = 2GM_{BH}/c_s^2$, where the sound speed c_s is estimated from X-ray observations of the gas temperature near the center of the galaxy. For 3C 84, as in most radio galaxies, this temperature is in the range 0.5–3 keV (Fabian et al. 2006), so the accretion radius is tens of parsecs. Our RM results and the free-free absorption data suggest, however, that accretion is disk-like on scales smaller than r_B, which implies that estimates of $\dot{M}_{BH}$ based on spherical Bondi or RIAF models may not be valid for all sources, especially those near the transition between RIAF and thin-disk accretion.

[9] Note that there is a typographical error in equation (9) of Marrone et al. (2006) – the power law index for r_{in} should be $-7/4$ (Macquart et al. 2006).

4.5. *Time variability*

On timescales of decades the emission from 3C 84 varies dramatically, both in the radio and in the γ-ray band; currently the source is brightening rapidly (Dutson et al. 2014), suggesting increased fueling of the black hole. Figure 1 in Dutson et al. (2014) shows that the 1.3 mm flux density increased by a factor of about 1.6 from mid-2011 to mid-2013. Over this same time span our polarization measurements show no apparent systematic increase in the RM. This suggests that processes inside r_{in} control accretion onto the black hole, or that our line of sight to the mm core does not pass through the inner accretion flow. More precise measurements of the RM would be valuable to search for variability caused by turbulence or patchiness in the accretion flow, as in the SgrA* models of Pang et al. (2011). Or, if the polarized mm emission originates in a hot spot moving outward along the radio jet, then changes in the RM could be used to probe the structure of the accretion flow as a function of radius.

5. SUMMARY

Polarization observations with CARMA and the SMA show that radio source 3C 84 is linearly polarized at wavelengths of 1.3 mm and 0.9 mm. The variation in position angle with wavelength is consistent with Faraday rotation, with a rotation measure of $(8.7 \pm 2.3)\times10^5$ rad m^{-2}, among the largest ever measured. The fractional polarization was 1–2% over most of the 2 years spanned by these observations. The rotation measure was stable within ±50% over this period, even as the polarization position angle drifted steadily toward more negative values, wrapping through a span of roughly 300 degrees.

We argue that at mm wavelengths the linearly polarized radiation from 3C 84 originates from the nucleus of the system, possibly within tens of Schwarzschild radii of the black hole, and that the Faraday screen lies just in front of the emission region. It is uncertain whether the Faraday rotation originates in in the boundary layer of the radio jet, or in the accretion flow onto the black hole. We investigated whether quasi-spherical radiatively inefficient accretion flow (RIAF) models could explain the measured RM but found that they overpredicted it by several orders of magnitude. This suggests that on scales of less than a parsec the accretion flow onto the black hole is primarily disk-like rather than spheroidal. The geometry of the disk previously inferred from free-free absorption appears to be correct, with the disk obscuring the counterjet and the innermost parts of the core.

More highly inclined systems such as Centaurus A may exhibit even larger RMs. Such sources would appear unpolarized in broadband observations. Spectropolarimetry at mm wavelengths with CARMA, SMA, and ALMA provides a powerful tool to uncover the accretion flows in these systems.

Support for CARMA construction was derived from the states of California, Illinois, and Maryland, the James S. McDonnell Foundation, the Gordon and Betty Moore Foundation, the Kenneth T. and Eileen L. Norris Foundation, the University of Chicago, the Associates of the California Institute of Technology, and the National Science Foundation. Ongoing CARMA development and operations are supported by the National Science Foundation under a cooperative agreement, and by the CARMA partner universities. DPM is supported by the National Science Foundation through award AST-1207752.

The Submillimeter Array is a joint project between the Smithsonian Astrophysical Observatory and the Academia Sinica Institute of Astronomy and Astrophysics, and is funded by the Smithsonian Institution and the Academia Sinica.

This study makes use of 43 GHz VLBA data from the VLBA-BU-BLAZAR Monitoring Program (VBUBMP; http://www.bu.edu/blazars/VLBAproject.html), funded by NASA through the Fermi Guest Investigator Program. The VLBA is an instrument of the National Radio Astronomy Observatory. The National Radio Astronomy Observatory is a facility of the National Science Foundation operated by Associated Universities, Inc.

Facilities: CARMA, SMA, Perkins.

REFERENCES

Allen, S. W., Dunn, R. J. H., Fabian, A. C., Taylor, G. B., & Reynolds, C. S. 2006, MNRAS, 372, 21
Aller, M. F., Aller, H. D., Hughes, P. A., & Latimer, G. E. 1999, ApJ, 512, 601
Asada, K., Kameno, S., Shen, Z.-Q., et al. 2006, PASJ, 58, 261
Bower, G. C., Wright, M. C. H., Falcke, H., & Backer, D. C. 2003, ApJ, 588, 331
Carilli, C. L., & Taylor, G. B. 2002, ARA&A, 40, 319
Conselice, C. J., Gallagher, III, J. S., & Wyse, R. F. G. 2001, AJ, 122, 2281
Doeleman, S. S., Fish, V. L., Schenck, D. E., et al. 2012, Science, 338, 355
Dutson, K. L., Edge, A. C., Hinton, J. A., et al. 2014, MNRAS, 442, 2048
Fabian, A. C. 1994, ARA&A, 32, 277
Fabian, A. C., Johnstone, R. M., Sanders, J. S., et al. 2008, Nature, 454, 968
Fabian, A. C., Sanders, J. S., Taylor, G. B., et al. 2006, MNRAS, 366, 417
Gardner, F. F., & Whiteoak, J. B. 1966, ARA&A, 4, 245
Hada, K., Doi, A., Kino, M., et al. 2011, Nature, 477, 185
Hull, C. L. H., Plambeck, R. L., Bolatto, A. D., et al. 2013, ApJ, 768, 159
Hull, C. L. H., Plambeck, R. L., Kwon, W., et al. 2014, ApJS, 213, 13
Jorstad, S. G., Marscher, A. P., Stevens, J. A., et al. 2007, AJ, 134, 799
Jorstad, S. G., Marscher, A. P., Larionov, V. M., et al. 2010, ApJ, 715, 362
Kuo, C. Y., Asada, K., Rao, R., et al. 2014, ApJ, 783, L33
Levinson, A., Laor, A., & Vermeulen, R. C. 1995, ApJ, 448, 589
Macquart, J.-P., Bower, G. C., Wright, M. C. H., Backer, D. C., & Falcke, H. 2006, ApJ, 646, L111
Marrone, D. P., Moran, J. M., Zhao, J.-H., & Rao, R. 2006, ApJ, 640, 308
—. 2007, ApJ, 654, L57
Marscher, A., Jorstad, S. G., Larionov, V. M., Aller, M. F., & Lähteenmäki, A. 2011, Journal of Astrophysics and Astronomy, 32, 233
Marscher, A. P. 2006, in American Institute of Physics Conference Series, Vol. 856, Relativistic Jets: The Common Physics of AGN, Microquasars, and Gamma-Ray Bursts, ed. P. A. Hughes & J. N. Bregman, 1–22
Marscher, A. P., Jorstad, S. G., D'Arcangelo, F. D., et al. 2008, Nature, 452, 966

Narayan, R., Sadowski, A., Penna, R. F., & Kulkarni, A. K. 2012, MNRAS, 426, 3241
Nemmen, R. S., & Tchekhovskoy, A. 2014, ArXiv e-prints, arXiv:1406.7420
Pang, B., Pen, U.-L., Matzner, C. D., Green, S. R., & Liebendörfer, M. 2011, MNRAS, 415, 1228
Sault, R. J., Teuben, P. J., & Wright, M. C. H. 1995, in ASP Conf. Ser. 77: Astronomical Data Analysis Software and Systems IV, Vol. 4, 433
Scharwächter, J., McGregor, P. J., Dopita, M. A., & Beck, T. L. 2013, MNRAS, 429, 2315
Shakura, N. I., & Sunyaev, R. A. 1973, A&A, 24, 337
Taylor, G. B., Gugliucci, N. E., Fabian, A. C., et al. 2006, MNRAS, 368, 1500
Trippe, S., Bremer, M., Krichbaum, T. P., et al. 2012, MNRAS, 425, 1192
Vermeulen, R. C., Readhead, A. C. S., & Backer, D. C. 1994, ApJ, 430, L41
Walker, R. C., Dhawan, V., Romney, J. D., Kellermann, K. I., & Vermeulen, R. C. 2000, ApJ, 530, 233
Walker, R. C., Romney, J. D., & Benson, J. M. 1994, ApJ, 430, L45
Wilman, R. J., Edge, A. C., & Johnstone, R. M. 2005, MNRAS, 359, 755
Zavala, R. T., & Taylor, G. B. 2004, ApJ, 612, 749